SLOPE STABILITY MONITORING USING SPACE-BORNE REPEAT-PASS SAR INTERFEROMETRY

Urs WEGMÜLLER[1], Charles WERNER[1], Tazio STROZZI[1], Andreas WIESMANN[1], and Hugo RAETZO[2]

[1] *Gamma Remote Sensing AG, Switzerland*

[2] *Federal Office for the Environment, Worblentalstrasse 68, CH-3063 Ittigen, Switzerland*

Abstract: A variation of the landslide activity is expected according to the climate change in the Alps, especially in permafrost environment. Mountain areas are not very well controlled by monitoring systems due to the high costs. Therefore, satellite data and especially repeat-pass SAR interferometric techniques are an important option for the monitoring.
In our contribution differential SAR interferometry and interferometric point target analysis are introduced. Based on examples of results the potential and limitations of these techniques are discussed.

1. INTRODUCTION

Over the last years mapping and monitoring of coherent displacements at c*m* to *mm* resolution with space-borne SAR interferometry reached some maturity. In Alpine terrain the application of the technique is particularly challenging but on the other hand for many alpine slopes the knowledge on the stability is quite minimal. Consequently, a novel method potentially providing such information is well received even if there are limitations to its applicability. This even more so, as space-borne SAR interferometry benefits from the already existing SAR data archives covering more than 15 years. The required interferometric SAR data are available from a number of space-borne SAR sensors including ERS-1, ERS-2, ENVISAT ASAR, Radarsat-1, JERS and ALOS PALSAR. At present data of additional sensors are becoming available (TerraSAR-X, Cosmo-Skymed, and Radarsat-2) and subsequent missions (including ESA Sentinels, follow-up Radarsat sensors) are being planned.

The two main product types generated are “land slide surveys”, i.e. products which are primarily used to identify unknown slope instabilities and to get information on the activity of known land-slides and “landslide monitoring”, providing quantitative and temporal information on the movements of specific landslides.

After a short review of the principles of SAR interferometry the main objective of this contribution will be to discuss potential and limitations of different methodologies and their dependence on system and scene parameters. For a more extensive introduction to SAR interferometry see the references Bamler et al., 1998 and Rosen et al., 2000.

2. DIFFERENTIAL INTERFEROMETRY (DINSAR)

2.1. DINSAR Methodology

In a complex-valued focused SAR image the phase corresponds to a sum of a term related to the return path of the signal and a term related to the arrangement of the scatterers in the resolution cell. For cells with many distributed scatterers this second part results in speckle with a spatially random phase in the interval [-π,π]. However, images acquired from almost the identical aspect angle, as shown in Figure 1, have almost identical speckle. Under such conditions the phase difference ϕ is related to the imaging path length difference

$$\phi = -\frac{4\pi}{\lambda}(|r_2| - |r_1|) \tag{1}$$

where λ is the radar signal wavelength. The phase is determined as the argument of the normalized interferogram, **γ**, defined as the normalized complex correlation coefficient of the complex backscatter intensities s_1 and s_2 at positions $\boldsymbol{r_1}$ and $\boldsymbol{r_2}$

$$\gamma = \frac{\langle s_2 s_1{}^* \rangle}{\sqrt{\langle s_1 s_1{}^* \rangle \langle s_2 s_2{}^* \rangle}} \tag{2}$$

with the brackets $\langle x \rangle$ standing for the ensemble average of x. The variance of the estimate of the interferometric phase $\hat{\phi}$ is reduced by coherent averaging over a set of looks, which are statistically independent samples of the resolution element. The degree of coherence, a measure of the phase noise, is defined as the magnitude of the normalized interferogram.

The interferometric imaging geometry formed by two passes of a radar sensor is separated by the baseline *B*. The precise look angle θ can be determined from the interferometric phase by solving for the cosine of the angle between the baseline vector and the look vector. The interferometric phase is sensitive to both surface topography and coherent displacement along the look vector occurring between the acquisition of the interferometric image pair. Inhomogeneous propagation delay ("atmospheric disturbance") and phase noise are the main error sources. The unwrapped interferometric phase ϕ_{unw} can be expressed as a sum of an orbital term ϕ_{orb}, a topographic term ϕ_{topo}, a displacement term ϕ_{disp}, a path delay heterogeneity term ϕ_{path}, and a phase noise (or decorrelation) term ϕ_{noise}:

$$\phi_{unw} = \phi_{orb} + \phi_{topo} + \phi_{disp} + \phi_{path} + \phi_{noise} \tag{3}$$

and with the expressions for the individual terms introduced:

$$\phi = \phi_{path} + \frac{4\pi}{\lambda}\frac{B_\perp}{r \cdot \sin\theta}h + \frac{4\pi}{\lambda}r_{disp} + \phi_{path} + \phi_{noise} \tag{4}$$

with the wavelength, λ and the baseline component perpendicular to the look vector, $B_\perp$, the incidence angle, θ, and the slant range, r. Changes in the atmospheric conditions (mainly water vapour) cause a variable path delay. In the microwave domain used, the path delay (expressed as a time delay) is independent of the radar frequency. As a consequence the path delay phase term is approximately proportional to the radar frequency. Spatial heterogeneity of ϕ_{path} results in the so-called atmospheric distortions, one of the main error sources in repeat-pass SAR interferometry.

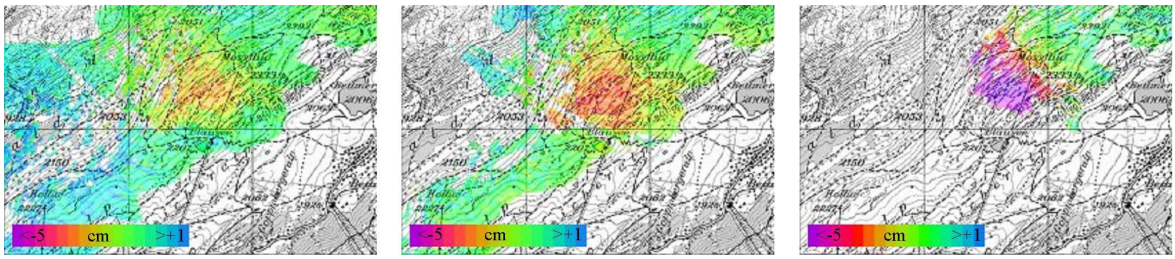

Figure 1 - Landslide above Aletsch glacier (Switzerland): displacement maps. Left: time interval of 105 days (ERS 16.07/29.10.99, 5 m). Middle: time interval of 351 days (ERS 10.08.95/26.07.96, 69 m). Right: time interval of 736 days (ERS 10.08.95/15.08.97, -19 m). The displacement is in the slant range direction. The negative sign indicates the direction away from the satellite (descending mode).

Random (or incoherent) displacement of the scattering centers as well as noise introduced by SAR signal noise is the source of ϕ_{noise}. Multi-looking and filtering of the interferogram reduce phase noise. The main difficulty with high phase noise is not so much the statistical error introduced in the estimation of ϕ_{topo} and ϕ_{disp} but resulting phase unwrapping problems. Ideally, the phase noise and the phase difference between adjacent pixels are both much smaller than π. In reality this is often not the case, especially for areas with a low coherence and rugged topography, as in the case of forested slopes, and for higher radar frequencies.

In differential interferometry the objective is to separate different phase components. In the so-called 2-pass approach the topographic phase component is estimated based on an available digital elevation model and subtracted from the interferogram. The phase of the resulting differential interferogram includes the deformation phase as the "main signal" and the atmospheric phase, phase noise, residual topographic phase, and residual orbital phase as the main error terms. If no DEM is available multi-pass differential interferometry can be used to still separate the topography and deformation related components. The basic idea here is to retrieve the height and deformation rate using pairs acquired with different time intervals and baselines. For further discussion of differential interferometric approaches it is referred to Wegmüller et al., 1998.

Pairs acquired with different acquisition intervals can be used to identify and quantify different deformation rates. Short intervals are better suited for fast deformations. Long intervals for slow deformations. Ideally, the movements cause differential interferometric phases between about π and 9π. For smaller values the accuracy is too low considering possible atmospheric distortions and for larger values phase unwrapping is often not possible due to too high phase gradients. To confirm a deformation signal multiple consistent observations should be used to reasonably exclude atmospheric artefacts, as shown in Figure 1 for a landslide above the Aletsch glacier, Switzerland. Displacement maps for time periods of 105, 351 and 736 days are presented. The LOS displacement observed nicely increases with increasing time interval.

2.2. DINSAR Examples

Alta Val Badia, Italy

The whole area of the Alta Val Badia region around Corvara (Figure 2) has important hazard for landslides (Soldati et al., 2004). At altitudes up to the tree line the slopes are covered by forests and meadows; above the tree line the vegetation gets sparse. A series of differential interferograms was computed for this area to identify slope instabilities. In Figure 3 two ERS

C-band differential interferograms are shown, both acquired with short baselines for a time interval of 35 days in late summer. JERS (Figure 4) and PALSAR (Figure 5) L-band differential interferograms over the same area are shown for acquisition time intervals of 88 days and 46 days, respectively. In the C-band interferograms high coherence is mainly observed above the tree line. Furthermore, a significant fraction of the total area is affected by layover (black areas in Figures 3-5) as a consequence of the steep 23 degree incidence angle of the ERS SAR. Using JERS-1 and PALSAR the layover area is smaller because of the larger incidence angle (38 degrees) and the coherence is higher because of the longer L-band wavelength, even for the forested areas. Furthermore, L-band is better suited in the case of strong deformation because of its lower phase to displacement sensitivity. In most of the cases, the signals related to the displacements observed with JERS and PALSAR interferometry are also visible with ERS data. However, at C-band (ERS) the noise is higher, preventing the correct unwrapping of the phase on a regional scale. Only for limited areas and after cautious phase filtering and masking of all residual signals, displacement maps could be computed with ERS interferometry. Instabilities identified in these differential interferograms are marked by white ellipses. The yellow ellips marks a specific landslide near Corvara, which was quantitatively analysed, validated and interpreted (see Belitz et al., 2003, Strozzi et al., 2005).

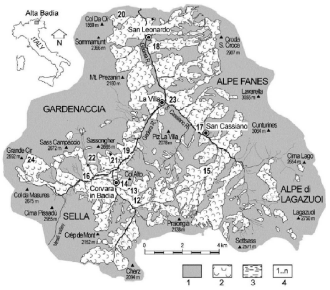

Figure 2 - Geomorphological sketch of Alta Val Badia (Corsini, 2002).

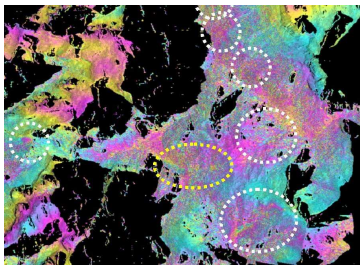

9.8. – 13.9.1997 (35 days, 76 m)

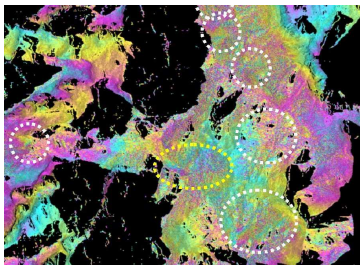

13.9. – 18.10.1997 (35 days, -85 m).

Figure 3 - Differential, filtered, geocoded ERS interferograms for two 35 day time intervals in 1997.

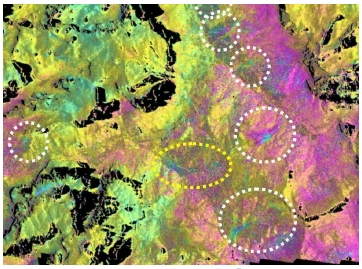

11.8. – 7.11. 1995 (88 days, 254 m)

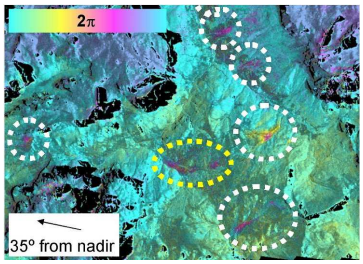

2.7. – 28.9.1998 (88 days, 217 m).

Figure 4 - Differential, filtered, geocoded JERS interferograms for 88 day periods in 1995 and 1997.

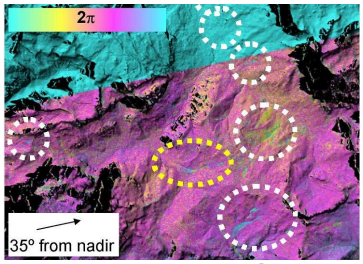

8.7. – 2.9.2007 (46 days)

Figure 5 - Differential, filtered, geocoded PALSAR interferogram for 46 day period in 2007.

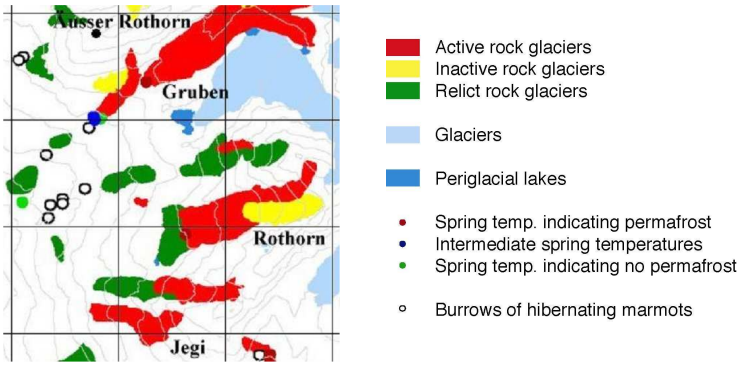

Figure 6 - Rock glacier inventory of the Fletschhorn region with glacier extent as in 1988 (Frauenfelder, 1997). The overlaid grid has a mesh of 1 km. Legend of the rock glacier inventory from in-situ natural indicators.

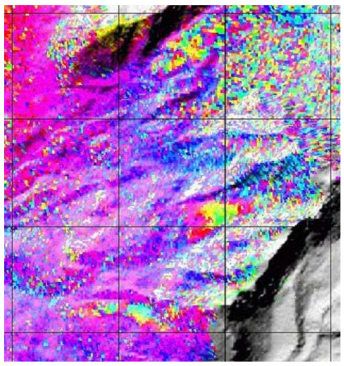

Figure 7 - Differential, filtered, geocoded JERS interferogram 21.6. – 17.9.1996 (88 days, -64m).

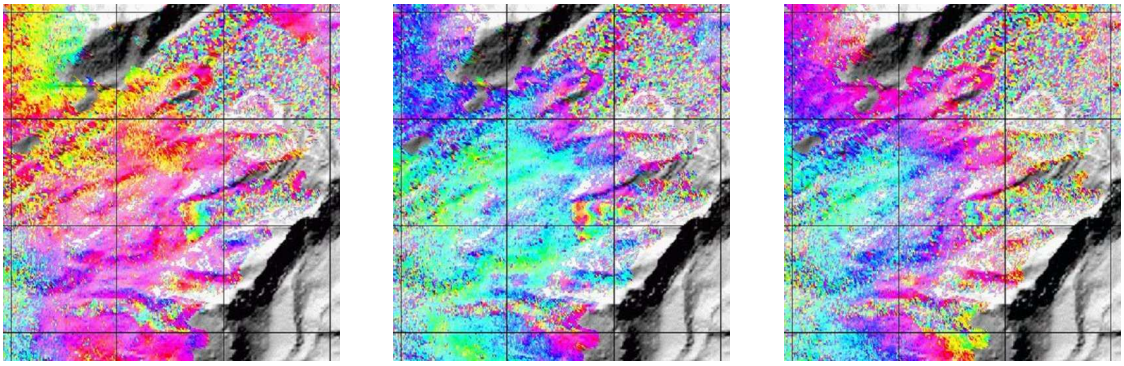

31.7.1998 – 4.9.1998, 35 days, 105.6 m. 16.7.1999 – 24.9.1999, 70 days, -108.8 m. 16.7.1999 – 29.10.1999, 105 days, 4.7 m.

Figure 8 - Differential, filtered, geocoded ERS interferograms over the Fletschhorn region superimposed to a shaded relief of the aerial photogrammetry DEM.

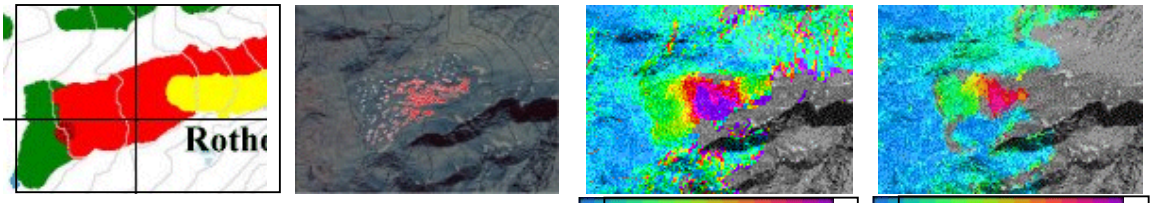

(a) Rothorn max 30 cm/year 1996.06.21_1996.09.17 JERS / 88 days / -64.5 m 1999.07.16_1999.09.24 ERS / 70 days / -108.8 m

Figure 9 - Surface displacement velocity over Rothorn rock glaciers in the Fletschhorn region. From left to right: extract of the rock glacier inventory by Frauenfelder, R. 1997., digital photogrammetry results by Kääb, 2002, with the arrows indicating the direction and magnitude of the displacements, JERS based deformation map, ERS based deformation map. For the DINSAR based results creeping in the direction of the maximum slope was assumed.

Permafrost creep and rock glaciers in Fletschhorn area Switzerland

Results for the Fletschhorn area in the Simplon/Saas valley region, Swiss Alps, were analyzed together with the survey of rock glaciers (see Figure 1 modified from Frauenhofer, 1997) and displacement maps from digital photogrammetry of repeated airborne imagery (Kääb, 2002). One JERS and three ERS differential interferograms are shown in Figures 7 and 8. A surface velocity map for a selected rock glacier is presented in Figure 9.

In all the interferograms of Figures 7 and 8 glaciated areas are completely decorrelated because of large displacements in the considered time intervals, the presence of wet snow, and surface ice melt. Two rock glacier systems may be immediately identified, Rothorn and Jegi. The phase signal over the Rothorn rock glacier is particularly clear in the JERS interferogram. For this large active rock glacier JERS DInSAR is able to display the entire flow field with the typical velocity distribution of highest speeds in the rock glacier center (see Figure 9). In the ERS interferograms the phase signal is clear only over the front of the rock glacier, where an increase of the fringes can be observed. The Jegi and the Gruben rock glaciers are more decorellated than the Rothorn one, suggesting larger creep velocities. For further discussion on this example see Strozzi et al., 2004.

3. PERSISTENT SCATTERER INTERFEROMETRY (PSI)

Over the last couple of years so-called Persistent Scatterer Interferometry (PSI) techniques were developed at several institutes and were applied in a significant number of cases (see e.g. TERRAFIRMA Project homepage: http://www.terrafirma.eu.com). GAMMA's PSI implementation is referred to as Interferometric Point Target Analysis (IPTA).

3.1. IPTA Methodology

Interferometric Point Target Analysis (IPTA) is a method to exploit the temporal and spatial characteristics of interferometric signatures collected from point targets to accurately map surface deformation histories, terrain heights, and relative atmospheric path delays.

The phase model used is identical to conventional differential interferometry. To use targets with point like scatter characteristics, only, has the advantage that there is much less geometric decorrelation for these targets. This permits phase interpretation even for large baselines above the critical one. Consequently, more image pairs may be included in the analysis improving the temporal sampling. Another important advantages is the potential to find scatterers in low-coherence areas permitting filling spatial gaps in the deformation maps. The point-like scatterers very often correspond to infrastructure as buildings, or other temporally rather stable targets as rocks. Due to their specific nature, targets with a point like scattering characteristics very often maintain coherence over long time periods. For a more detailed discussion of the IPTA technique see Werner et al., 2003, or Wegmüller et al., 2004.

The most straightforward application of IPTA is the monitoring of slow and temporally uniform deformation. In this case the temporal and spatial sampling of the signal is very good. In the case of higher deformation rates the capability of the point target based interferometric technique to use pairs with large baselines has the advantages that high phase gradients can be reduced if shorter observation intervals become available. In addition, large scale corrections such as baseline errors and the large scale component of the atmospheric distortions can be estimated independently of the areas with high deformation gradients and interpolated or extrapolated to get relatively accurate corrections for the entire area. The spatial separation of the available point-like scatterers is of course an important factor. Larger distances, i.e. lower spatial sampling, strongly reduces the potential to resolve high phase gradients. In the case of temporally strongly varying deformation rates spatial unwrapping of the phases is necessary.

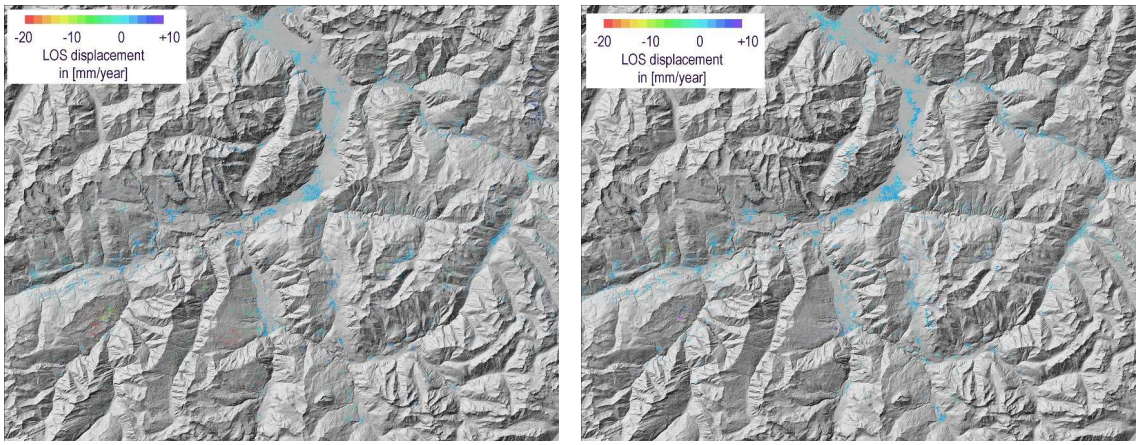

Figure 10 - Average deformation rates 1992-2005 derived from ascending track 215 (left) and descending track 480 (right) ERS and ENVISAT over Grison, using IPTA, superimposed to shaded relief.

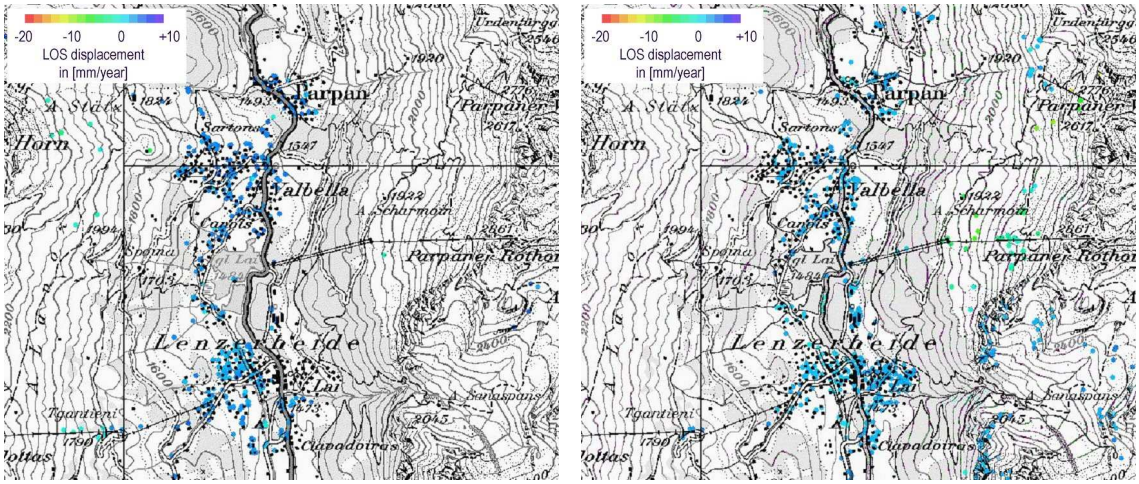

Figure 11 - Detailed view of Grison inventory result (Figure 10) for Lenzerheide. The ascending track result (left) is well suited for the valley slope to the West, the descending track result (right) for the valley slope to the East.

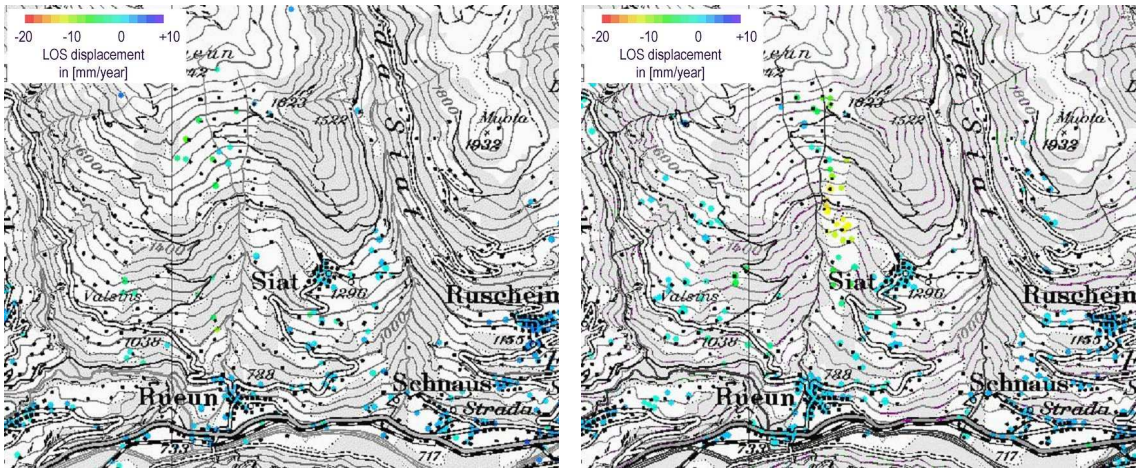

Figure 12 - Detailed view of Grison inventory result (Figure 10). The ascending track (left) and descending track (right) results indicate slope movements above Rueun.

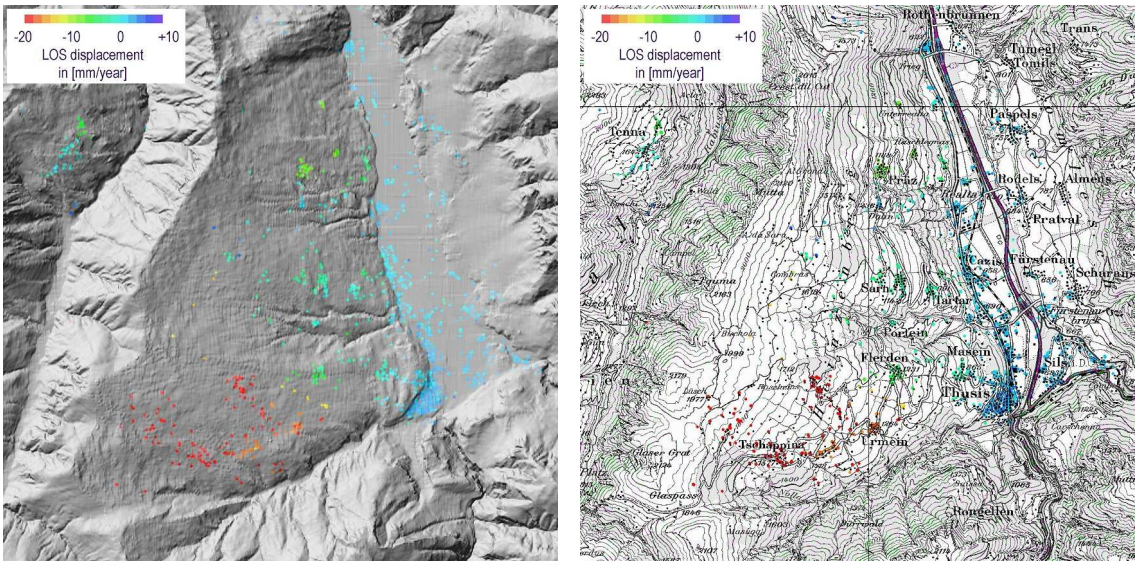

Figure 13 - Monitoring result for Heinzenberg. The average deformation rate 1992-2005 is superposed to the shaded relief (left) and to the topographic map (right). Ascending track ERS and ENVISAT data were used. For each point shown the deformation history was derived.

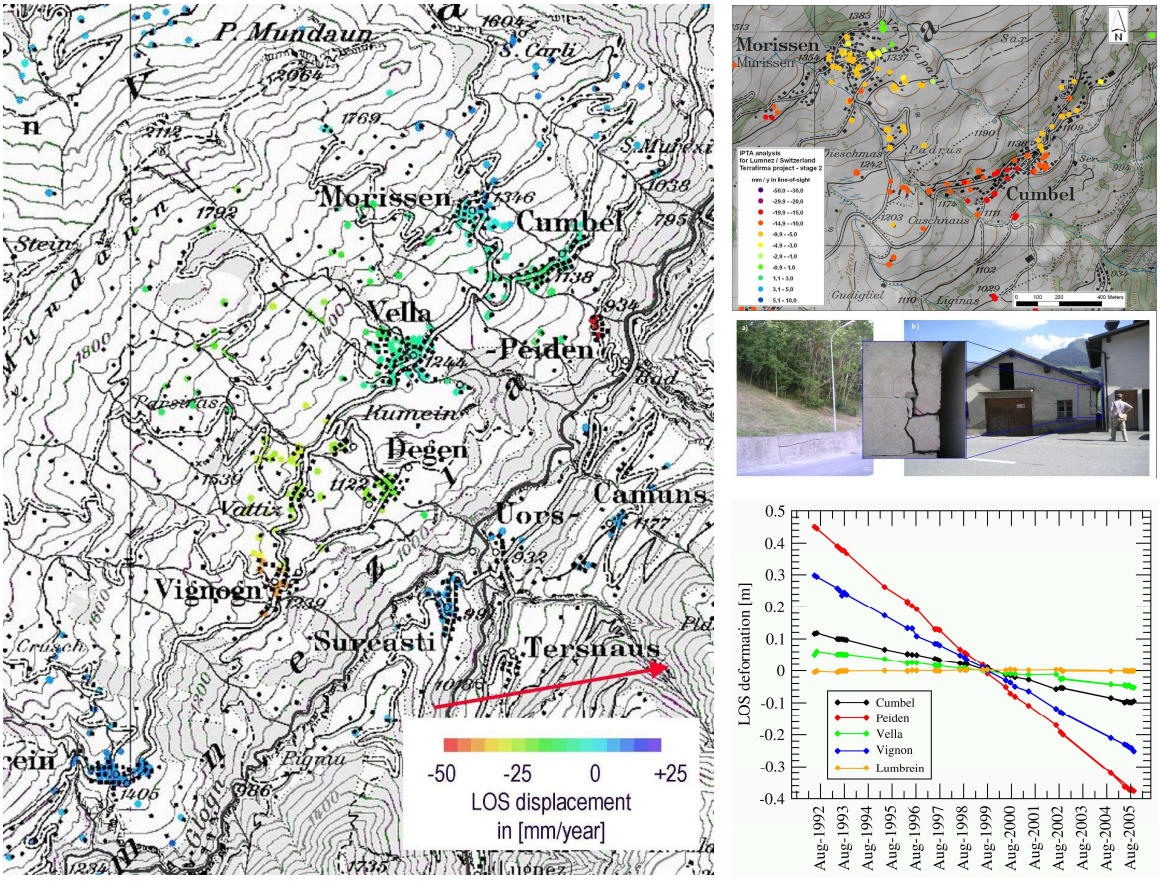

Figure 14 - Monitoring result for Lumnez. The average deformation rate is for 1992-2005. Ascending track ERS and ENVISAT data were used. Line-of-sight deformation rates up to 7cm/year were retrieved.

3.2. IPTA Examples

Landslide inventories are one important IPTA result. The main objective of the inventory is to identify for a larger area unknown slope instabilities and to determine for known landslides the activity. Often, both ascending and descending orbit data are considered to improve the overall spatial coverage. An landslide inventory product for a 4000 km^2 area in the Canton Grison, Switzerland is shown in Figure 10. It is worth noting than in general forested areas are not covered with IPTA information. Also over alpine areas above the tree line there are generally no points because acquisitions with snow cover at high altitudes were included in the analysis to improve the temporal sampling of the landslides at lower altitudes. Details of the result, superimposed to a topographic map, are shown in Figures 11 and 12. For some of the main known landslides in the area a more detailed monitoring was conducted. For Heinzenberg the deformation rate is shown superimposed to the shaded relief and superimposed to the map (Figure 13). For Lumnez the average rate is shown as well as deformation histories for points in some of the villages (Figure 14).

4. DISCUSSION AND CONCLUSIONS

Landslide survey and monitoring results obtained over different alpine sites were presented. The examples shown clearly confirm the potential of the space-borne SAR interferometric techniques for the identification, mapping and monitoring of alpine ground movements. The DINSAR approach is particularly well suited for areas above the tree-line. Depending on the motion rates pairs covering different time intervals are most useful. At C-band the applicability is good for displacements between about 5mm and 10cm during the acquisition interval. In the archives pairs for one day intervals (ERS-1/2 Tandem pairs) as well as for longer intervals (e.g. multiples of 35 days for ENVISAT) are available. At L-band the applicability is good for displacements between about 2cm and 40cm during the acquisition interval. The shortest interval pairs are 44 day intervals (JERS-1). Longer intervals (e.g. multiples of 46 days for PALSAR) are available as well. At L-band a better spatial coverage is achieved partly thanks to the higher incidence angle and partly because of the reduced decorrelating influence of the vegetation scattering.

The IPTA requires quite significant data stacks. When such stacks are available reliable deformation rates are retrieved mainly for areas with some infrastructure or other hard targets as larger rocks. Reliable results are usually obtained for all villages. At higher altitudes some spatial coverage is achieved as there are often still some individual buildings, as well as other infrastructure (e.g. ski-lifts, power-lines etc.). For deformation rates up to about 2cm/year the accuracy achieved is typically high in the order of 1mm/year. At higher rates it becomes more difficult to retrieve a reliable result. Nevertheless, the examples show also some cases where we successfully mapped faster deformations.

In some cases the results could be validated with auxiliary information and in other cases an independent interferometric analysis conducted using alternative data over the same area gave additional confidence in the results.

Considering the high costs related to landslide mapping, and in particular the difficulties in the detection of the active, slow, and dormant parts of landslides, the use of a SAR interferometry based approach can positively impact on the hazard mitigation activities of local and regional authorities.

Acknowledgments

The present work was supported by the European Space Agency in the framework of the projects "GSE Terrafirma", "SLAM", "Alps", "ALPSLOPE", and by the Federal Office for the Environment (FOEN), and by the EC FP6 Project "ASSIST". ERS and ENVISAT SAR data were provided by ESA, partially as part of CAT-1 projects. JERS and PALSAR data were provided by JAXA and ESA AO Projects. DEM 2000 (courtesy of Provincia Autonoma di Bolzano-Alto Adige, Ufficio Coordinamento Territoriale) and DHM25 (© 2003 swisstopo) were used as height references in the analysis.

References

Bamler R. and P. Hartl, "Synthetic aperture radar interferometry," Inverse Problems, no. 14, pp. R1-R54, 1998.

Belitz K., A. Corsini, V. Mair, T. Strozzi, U. Wegmüller, and J. Zilger, "Support of satellite radar to hazard zone mapping in the Italian Alps," *Proceedings of FRINGE 2003*, ESA ESRIN, Frascati, Italy, 1-5 December 2003.

Corsini A., A. Pasuto, M. Soldati and A. Zannoni, "Researches for landslide hazard assessment in the area of Corvara in Badia (Dolomites, South Tyrol, Italy): a summary overview," in L. Borgatti and M. Soldati (eds.), Relationships between man and the mountain environment in terms of geomorphological hazard and human impact in Europe, *IAG Symposium Proceedings*, Dornbirn (Austria), pp. 59-60, 14 July 2002.

Frauenfelder, R. 1997. Permafrostuntersuchungen mit GIS - Eine Studie im Fletschhorngebiet. Master-Thesis, Department of Geography, University of Zurich: 77.

Kääb, A. 2002. Monitoring high-mountain terrain deformation from digital aerial imagery and ASTER data. ISPRS Journal of Photogrammetry and remote sensing, 57(1-2): 39-52.

Rosen P., S. Hensley, I. Joughin, F. Li, S. Madsen, E. Rodriguez, and R. Goldstein, "Synthetic Aperture Radar Interferometry," *Proceedings of the IEEE*, Vol. 88, No. 3, pp. 333-382, March 2000.

Soldati M., A. Corsini and A. Pasuto, "Landslides and climate change in the Italian Dolomitessicen the Late glacial," *Catena*, Vol. 55, pp. 141-161, 2004.

Strozzi T., L. Tosi, L. Carbognin, U. Wegmüller and A. Galgaro, "Monitoring Land Subsidence in the Euganean Geothermal Basin with Differential SAR Interferometry," *Proceedings of FRINGE'99*, Liège, Belgium, 10-12 November 1999, ESA Publication SP-478.

Strozzi T., A. Kääb and R. Frauenfelder, Detecting and quantifying mountain permafrost creep from in situ inventory, space-borne radar interferometry and airborne digital photogrammetry, Int. J. Remote Sensing, Vol. 25, No. 15, pp. 2919-2931, doi: 10.1080/0143116042000192330 2004.

Strozzi T., P. Farina, A. Corsini, C. Ambrosi, M. Thüring, J. Zilger, A. Wiesmann, U. Wegmüller and C. Werner, Survey and monitoring of landslide displacements by means of L-band satellite SAR interferometry, Landslides, Vol. 2, No. 3, pp. 193 – 201, doi: 10.1007/s10346-005-0003-2, 2005.

Tosi, L. L. Carbognin, P. Teatini, T. Strozzi, and U. Wegmüller, Evidence of the present relative land stability of Venice, Italy, from land, sea, and space observations, AGU Geophysical Research Letters, Vol. 29, No. 12, 18. Jun. 2002, (10.1029/2001GL013211).

Wegmüller U., and T. Strozzi, Characterization of differential interferometry approaches, EUSAR'98, 25-27 May, Friedrichshafen, Germany, VDE-Verlag, ISBN 3-8007-2359-X, pp. 237-240, 1998.

Wegmüller U., C. Werner, T. Strozzi, and A. Wiesmann, "Multi-temporal interferometric point target analysis", in Analysis of Multi-temporal remote sensing images, Smits and Bruzzone (ed.), Series in Remote Sensing, Vol. 3, World Scientific (ISBN 981-238-915-61), pp. 136-144, 2004.

Werner C, U. Wegmüller, T. Strozzi, and A. Wiesmann, "Interferometric Point Target Analysis for Deformation Mapping," *Proceedings of IGARSS'03*, Toulouse, France, 21-25 July, 2003.

Corresponding author contacts

Urs Wegmüller, wegmuller@gamma-rs.ch
GAMMA Remote Sensing AG, Worbstrasse 225, 3073 Gümligen, Switzerland
Tel: +41 31 9517005, Fax: +41 31 9517008
Hugo RAETZO
Federal Office for the Environment, Worblentalstrasse 68, CH-3063 Ittigen, Switzerland